Science of the Total Environment 574 (2017) 716–723

Contents lists available at ScienceDirect

Science of the Total Environment

journal homepage: www.elsevier.com/locate/scitotenv

Study of the water transportation characteristics of marsh saline soil in the Yellow River Delta

Fuhong He [a], Yinghua Pan [a,*], Lili Tan [a], Zhenhua Zhang [a,*], Peng Li [a], Jia Liu [a], Shuxin Ji [a], Zhaohua Qin [a], Hongbo Shao [b,c,*], Xueyan Song [a]

[a] School of Resources and Environmental Engineering, Ludong University, Yantai 264025, China
[b] Institute of Agro-biotechnology, Jiangsu Academy of Agricultural Sciences, Nanjing 210014, China
[c] Yantai Institute of Coastal Zone Research, Chinese Academy of Sciences, Yantai 264003, China

HIGHLIGHTS

- Cumulative infiltration capacity increased with the depth of the soil layers.
- Initial rates of capillary rise were lower than the initial infiltration rates.
- Water transportation of wetland saline soil accords to common principle.
- Plant type may be the main factor which influences water and salt transportation.

GRAPHICAL ABSTRACT

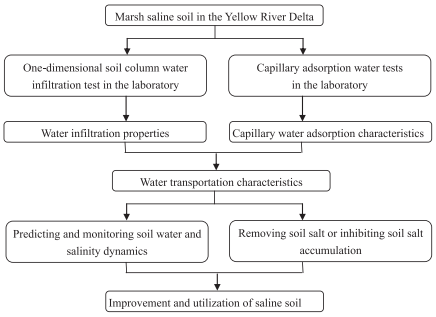

Flow chart of improvement and utilization of saline soil

ARTICLE INFO

Article history:
Received 30 June 2016
Received in revised form 13 September 2016
Accepted 14 September 2016
Available online 14 October 2016

Editor: D. Barcelo

Keywords:
Accumulative infiltration capacity
Infiltration rate
Accumulative capillary adsorbed water volume
Capillary rise rate
Marsh saline soil

ABSTRACT

One-dimensional soil column water infiltration and capillary adsorption water tests were conducted in the laboratory to study the water transportation characteristics of marsh saline soil in the Yellow River Delta, providing a theoretical basis for the improvement, utilization and conservation of marsh saline soil. The results indicated the following: (1) For soils with different vegetation covers, the cumulative infiltration capacity increased with the depth of the soil layers. The initial infiltration rate of soils covered by *Suaeda* and *Tamarix chinensis* increased with depth of the soil layers, but that of bare soil decreased with soil depth. (2) The initial rate of capillary rise of soils with different vegetation covers showed an increasing trend from the surface toward the deeper layers, but this pattern with respect to soil depth was relatively weak. (3) The initial rates of capillary rise were lower than the initial infiltration rates, but infiltration rate decreased more rapidly than capillary water adsorption rate. (4) The two-parameter Kostiakov model can very well-simulate the changes in the infiltration and capillary rise rates of wetland saline soil. The model simulated the capillary rise rate better than it simulated the infiltration rate. (5) There were strong linear relationships between accumulative infiltration capacity, wetting front, accumulative capillary adsorbed water volume and capillary height.

* Corresponding authors.
E-mail addresses: panxingxing@126.com (Y. Pan), zhangzh@163.com (Z. Zhang), shaohongbochu@126.com (H. Shao).

http://dx.doi.org/10.1016/j.scitotenv.2016.09.111
0048-9697/

1. Introduction

The Yellow River Delta possesses abundant natural resources and plays an important role in the social and economic development, ecological environment construction and conservation in China. The formation time of soil in the Yellow River Delta is relatively short. The soil mainly consists of sediment. However, due to the shallow underground water table and a large ratio of evaporation to precipitation, secondary soil salinealkalization is likely to occur. Evaporation and infiltration are two opposite processes of soil water transportation, which are also important processes impacting salt accumulation and eluviation of saline soil. Under evaporation, soil capillary action causes salt to move from deeper soil layers to the surface along with moving water. The salt was retained at the soil surface after the water was evaporated. When precipitation or irrigation occurs, water transports salt at the soil surface to deeper layers, which decreases the salt concentration at the soil surface. The extent of salt leaching and water evaporation is closely related to soil water infiltration properties, water adsorption capability of capillary and soil water conductivity. Infiltration and capillary adsorption are important processes of water transportation in saline soil. Therefore, understanding soil water transportation characteristics, predicting and monitoring soil water and salinity dynamics, and removing soil salt or inhibiting soil salt accumulation in a timely manner to reduce its damage to plants are important practices of soil improvement and utilization in this region.

Soil water movement was influenced by various factors, such as soil particle composition, soil mineral composition (Frenkel et al., 1978), soil structure, cultivation modes (Pardini et al., 2003), soil organic matter (Barzegar et al., 2002), plant cover (Turrion et al., 2007), irrigation water quality (So and Aylmore, 1993; Ayars et al., 1993; Moutier et al., 1998; Bagarello et al., 2006; Bardhan et al., 2016) and soil salt content (Crescimanno et al., 1995; Suarez, 2006a, b; Quirk and Schofield, 2013). There were plenty of studies about the effects and mechanism of different factors on water movement in non-saline-alkaline soil (Shao and Horton, 1999; Yan et al., 2007; Wu and Wang, 2007). Among these publications, there was an extensive series of scientific reports on the effects of waters of varying quality on soil hydraulic properties. Agassi et al. (1981) determined that the infiltration rate was more sensitive to the effects of sodicity when applying the water via rainfall simulator compared with changes in hydraulic conductivity in saturated column studies. These differences were attributed to particle disturbance on the soil surface. Kazman et al. (1983) used disturbed soil prepared at various ESP values, packed in soil trays and leached with a rainfall simulator. The results showed that infiltration rate decreased as the ESP increased. Suarez et al. (2006a) examined water infiltration into loam and clay soils irrigated at EC = 1.0 and 2.0 dSm^{-1} at SAR of 2, 4, 6, 8, and 10 in a management system with alternating (simulated) rain and irrigation and drying between irrigations. The results showed a greater sensitivity to SAR than indicated in laboratory column studies and existing water quality criteria.

In terms of the infiltration properties of saline and alkaline soil, most studies focus on soils in arid and semi-arid regions (Shi et al., 2007). The formation mechanism of saline-alkaline soil in arid and semi-arid regions are different from that in the Yellow River Delta. The main formation mechanism of saline-alkaline soil in arid and semi-arid regions is that underground water rises to the soil surface in association with atmospheric evaporation, whereas the formation of saline soil in the Yellow River Delta is due to secondary saline-alkalization. Therefore, the improvement of saline-alkaline soil in the Northwest region of China is mainly to inhibit evaporation and reduce salt accumulation at the surface, whereas the improvement in the Yellow River Delta includes evaporation inhibition in the dry seasons and increasing leaching and salt elimination in the rainy seasons. For saline-alkaline soil, whether through inhibiting evaporation or elimination of salt, understanding soil hydraulic properties and monitoring the water and salt dynamics are an important basis for taking proper measures of soil improvement (Churchman et al., 1993; Levy et al., 2005; Zhang et al., 2007; Jayawardane et al., 2011).

Based on the analysis mentioned above, the present paper aims to study: (1) the water infiltration properties of marsh saline soil in the Yellow River Delta; (2) the capillary water adsorption characteristics of marsh saline soil; (3) dynamic simulation of infiltration and capillary adsorption; and (4) the relationship between one-dimensional water infiltration processes and the capillary adsorption process.

2. Materials and methods

The soil samples were taken from the Ecology Experimental Station of the Chinese Academy of Science in Yellow River Delta Coastal Wetland. The experimental station is located in Kenli County of Dongying City in Shandong Province of China (37°45′36.32″ to 37°46′15.56″N, 18°58′38.74″ to 118°58′58.77″E). Usually, plants can reflect the soil qualities and some soil physical and chemical properties (Turrion et al., 2007). So, at the station, lands with three typical types of vegetation cover were selected, including *Tamarix chinensis*, *Suaeda* and bare land. For each vegetation cover type, three soil sampling plots were randomly selected and sampled by layers. The sampling depth of *Suaeda glauca* (*Bunge*) Bunge. covered land and bare land were both 0–50 cm. Because of the waterlogged conditions *Tamarix chinensis* covered land, the sampling depth was 0–30 cm. All soil samples were taken at intervals of 10 cm in terms of depth, then air dried and sieved through 1 mm griddle. The basic properties of different soil profile layers are shown in Table 1. Seen from Table 1, for three vegetation covered soils, sand content was the highest, followed by the silt content, and the clay content is the lowest. According to the international soil classification standard, three-type vegetation covered soils are all sandy loam. According to electrical conductivity (EC), pH and total salt content, the soil in this region belongs to typical saline soil. The salt content is highest on the surface of bare land and decreases with depth, reaching a stable value at depths of 30–50 cm. The salt content is relatively low at the surface layer of soil covered by *Suaeda glauca* (*Bunge*) Bunge. and insignificantly increases with depth. The salt content is high at the surface layer of *Tamarix chinensis* covered soil and decreases with depth. Within 0–30 cm depth, the total soil salt contents in three vegetation covered soils differed greatly, and the total salt contents of bare soil in all layers are higher than those in other two types of soil.

In the laboratory, to ensure the same basic soil conditions, disturbed soil column experiments were carried out to study the water transportation characteristics of marsh saline soil. Two types of experiments were carried out: one-dimensional constant head water ponding infiltration and investigation of capillary water adsorption capability. The experimental soil columns were 5.4 cm in inner diameter and 20 cm high. Soil was packed in the columns layer-by-layer (2 cm at a time), and the bulk density was approximately 1.35 g/cm^3. Water heads were 1 cm for one-dimensional water ponding infiltration, controlled by Mariotte flask. In the capillary water adsorption ability tests, soil columns were placed on sand (2–3 cm in diameter) surface in beakers Before the experiment, sand in beakers was cleaned by diluted hydrochloric acid and pure water to prevent the adsorption and infiltration of other salt ions and their potential effects on the final results. The sand in the beakers was submerged to simulate the underground water interface of soil profiles under natural conditions. The outlet of the Mariotte flask was kept in line with the sand surface, and placed soil columns on the sand surface. After the experiment began, the water infiltration capacity and advancing distance of wetting front were recorded.

3. Results and discussion

3.1. Analysis of the water transportation characteristics in marsh saline soil profiles

3.1.1. Infiltration properties in soil profiles under one-dimensional water ponding infiltration with constant head

Figs. 1, 2 and 3 showed the dynamic processes of accumulative infiltration and infiltration rate of *Tamarix chinensis* Lour. covered and

Table 1
Basic properties of the studied soil.

Plant cover	Soil layer (cm)	Sand (%)	Silt (%)	Clay (%)	Electrical conductivity (mS/cm)	pH	Total salt content (g/kg)
		2–0.02 mm	0.02–0.002 mm	<0.002 mm			
Bare land	0–10	69.91 ± 3.46bc	25.53 ± 3.17a	4.56 ± 0.29ab	6.80 ± 0.74a	7.75 ± 0.17a	28.21 ± 1.52a
	10–20	67.31 ± 1.72c	27.55 ± 1.56a	5.14 ± 0.18a	5.07 ± 0.63b	7.62 ± 0.27a	18.59 ± 0.90b
	20–30	72.80 ± 2.15b	23.13 ± 1.84a	4.07 ± 0.50b	4.15 ± 0.72bc	7.83 ± 0.03a	16.30 ± 1.13c
	30–40	80.39 ± 1.64a	16.65 ± 1.54b	2.96 ± 0.17c	3.17 ± 0.39c	7.81 ± 0.09a	11.29 ± 0.48d
	40–50	81.42 ± 1.38a	15.81 ± 1.33b	2.77 ± 0.06c	3.01 ± 0.44c	7.85 ± 0.10a	11.18 ± 0.60d
Suaeda glauca (*Bunge*) Bunge.	0–10	79.81 ± 5.00ab	22.01 ± 4.08ab	4.13 ± 0.93a	2.76 ± 0.43b	7.16 ± 0.06c	9.81 ± 0.40a
	10–20	81.21 ± 1.49a	24.35 ± 1.32a	4.39 ± 0.19a	3.14 ± 0.25ab	7.46 ± 0.07b	10.56 ± 1.21a
	20–30	74.76 ± 2.21bc	21.51 ± 1.74ab	3.73 ± 0.47ab	3.59 ± 0.24a	7.45 ± 0.04b	12.58 ± 1.43a
	30–40	71.26 ± 0.63c	15.92 ± 0.63c	2.86 ± 0.05b	3.25 ± 0.48ab	7.66 ± 0.02a	12.55 ± 2.04a
	40–50	73.87 ± 0.51bc	17.29 ± 0.43bc	2.90 ± 0.10b	2.98 ± 0.12ab	7.62 ± 0.02a	11.25 ± 0.80a
Tamarix chinensis Lour.	0–10	73.55 ± 0.56c	22.35 ± 0.60a	4.10 ± 0.13a	4.31 ± 0.24a	7.22 ± 0.02b	15.38 ± 2.45a
	10–20	75.20 ± 0.58b	20.90 ± 0.58b	3.90 ± 0.10a	3.51 ± 0.04b	7.37 ± 0.08ab	12.41 ± 1.25a
	20–30	78.94 ± 0.69a	17.77 ± 0.46c	3.28 ± 0.28b	3.48 ± 0.38b	7.51 ± 0.05a	11.12 ± 1.00a

a: $P < 0.01$; b: $P < 0.05$; c: no obvious difference.

Suaeda glauca (*Bunge*) Bunge. covered soil and bare land soil, respectively. Fig. 1a showed that accumulative infiltration differed greatly in layers of the *Tamarix chinensis* Lour. covered soil. Accumulative infiltration of 20–30 cm deep layer was the greatest, followed by 10–20 cm and 0–10 cm soil layers. The dynamic change of infiltration rate (Fig. 1b) showed that within the initial 1 min, the average infiltration rate was 1.1 cm/min at 20–30 cm deep layer, 0.62 cm/min and 0.80 cm/min at 0–10 cm and 10–20 cm deep layer respectively then it decreased sharply. Ten minutes later, the infiltration rate decreased to 0.16 cm/min at 0–10 cm deep layer, 0.1 cm/min and 0.15 cm/min at 10–20 cm and 20–30 cm depth layer. The initial 10 min of infiltration process is the period when infiltration rate decreased very quickly and it also was the stage of quick increase of infiltration capacity. Thereafter, the infiltration rate declined gradually and reached a stable value within 0.02–0.03 cm/min at 34–37 min. The infiltration rate trends of three soil layers were more or less the same. Each change point of accumulative infiltration capacity was consistent with that of infiltration rate. The accumulative infiltration capacity generally increased with time. But at the key stage of infiltration rate change, increasing trend of accumulative infiltration was obvious and showed linear increasing tend after the infiltration rate achieved stable.

For *Suaeda glauca* (*Bunge*) Bunge. covered soil, the accumulative infiltration of 10–20 cm soil layer was the highest, 0–10 cm soil layer's was the lowest, 20–30 cm soil layer's was in the middle and it was negligibly different from that of the 0–10 cm soil layer (Fig. 2a). Although the accumulative infiltration of 10–20 cm layer was the highest, the error bars in the figure indicate a large difference among the three replicates. A much smaller difference was observed among the replicates in the other two soil layers (Fig. 2a). The dynamic infiltration rates of different soil layers showed (Fig. 2b) that the infiltration rates declined rapidly during the initial 10 min and declined slowly thereafter. The infiltration rate of the 0–10 cm soil layer reached a stable value at 25–28 min. The infiltration rates of other two soil layers became stable at 34–37 min. The stable infiltration rates of the three soil layers ranged within 0.2–0.3 cm/min and showed a similar trend.

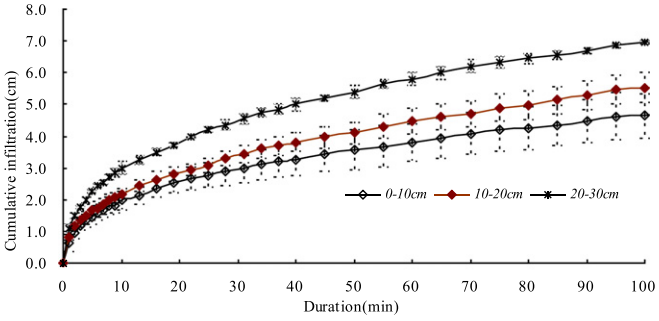

（a）Accumulative infiltration

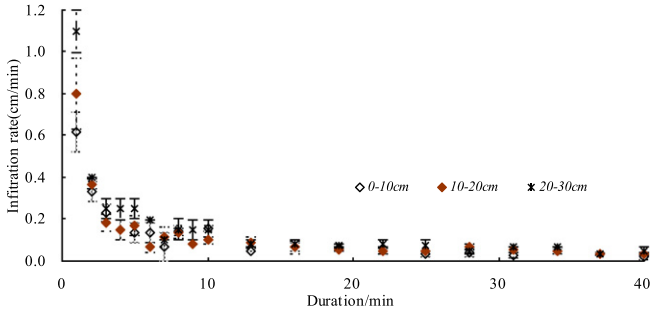

（b）Infiltration rate

Fig. 1. Dynamic accumulative infiltration capacity and infiltration rate of soil covered by *Tamarix chinensis* Lour.

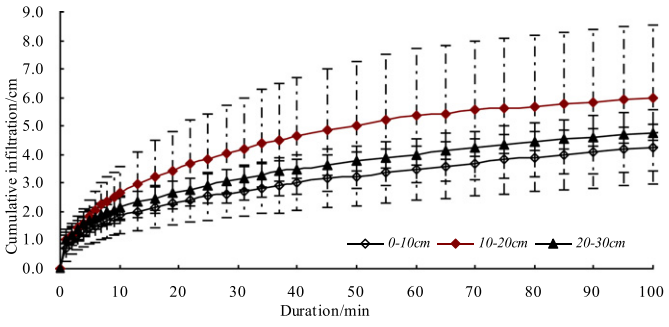

(a) Accumulative infiltration

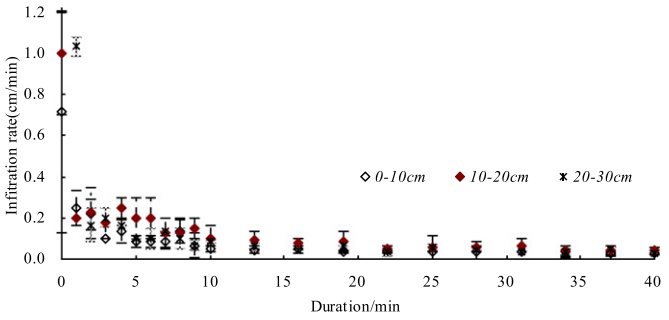

（b）Infiltration rate

Fig. 2. Dynamic accumulative infiltration capacity and infiltration rate of soil covered by *Suaeda glauca* (*Bunge*) Bunge.

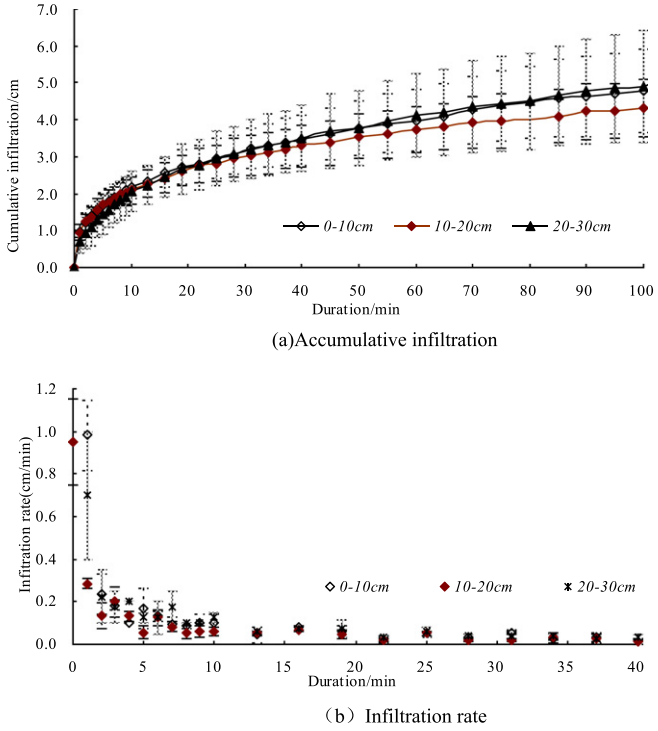

Fig. 3. Dynamic accumulative infiltration capacity and infiltration rate of bare land.

Fig. 3a shows the dynamic change of accumulative infiltration at different soil layers of bare land. It shows that there was no difference in the accumulative infiltration capacity of the 0–10 cm and 20–30 cm soil layers. The accumulative infiltration of the 10–20 cm soil layer was not different from that of the other two layers during the beginning-middle infiltration stages, and it varied gradually but not significantly during 13 to 19 min. The dynamic change of infiltration rate (Fig. 3b) showed that the infiltration rate was high in the 0–10 cm and 10–20 cm layers and low in the 20–30 cm layer. The infiltration rate of the 0–10 cm layer decreased from 0.95 cm/min to 0.13 cm/min within 6 min, that of the 10–20 cm layer decreased to 0.12 cm/min within 7 min, and that of the 20–30 cm layer decreased to the same level within 10 min. After the fast decline period, the decrease in the infiltration rate slowed and became stable at 30–37 min.

The changes of accumulative infiltration and infiltration rate of different plant cover soil layers showed that the infiltration properties may be influenced by soil salt content, soil texture and other factors relative to physiological and ecological habits of halophyte (Callaghan et al., 2014). For different soils under different plant cover, these factors may play different role in affecting soil infiltration properties We listed accumulative infiltration, infiltration rate and total salt content in Table 2. Accumulative infiltration and initial infiltration rate of soil covered by *Tamarix chinensis* Lour. increased with salt content decreasing. Infiltration rate of soil covered by *Suaeda glauca* (*Bunge*) Bunge. did not show a discernable pattern with the soil depth. The reasons may be that high sand contents and low clay contents in the 20–30 cm layer (Table 1) may contribute to the high infiltration rate in the 20–30 cm soil layer and infiltration rate in each soil layer did not increase constantly with sand content, which could be impacted by the soil salt content. If there was salt in the soil, the combined effects of the salt content and the soil mechanical composition may result in infiltration rate not fully following consistent regularity (Abu-Sharar et al., 1987; Reading, et al., 2012).

Fig. 4 shows the dynamic change of accumulative infiltration of different vegetation covered soils. Fig. 4a compares the accumulative infiltration of the 0–10 cm soil layers. The fast increase in the accumulative infiltration of soils covered by *Tamarix chinensis* Lour. and bare land during the earlier stages reflects its high infiltration rate and strong infiltration capacity. During the initial stage, the accumulative infiltration capacity of bare land increased faster than that of soil covered by *Suaeda glauca* (*Bunge*) Bunge. and *Tamarix chinensis* Lour. The accumulative infiltration change trend of *Tamarix chinensis* Lour. covered soil was the same as that of the bare land soil. After 10 min, the accumulative infiltration of soil covered by *Tamarix chinensis* Lour. was significantly higher than that of soil covered by *Suaeda glauca* (*Bunge*) Bunge. Approximately 20 min later, the three curves of the accumulative infiltration capacity became nearly parallel, indicating stable and similar infiltration rates for the three vegetation cover types. Fig. 4b shows the dynamic change of accumulative infiltration of the 10–20 cm soil layer. There were no appreciable differences among the three vegetation cover types at 0–5 min. A significant difference occurred after 5 min. The accumulative infiltration capacity of bare land was clearly lower than that of soil covered by *Tamarix chinensis* Lour. and *Suaeda glauca* (*Bunge*) Bunge. after 10 min. The accumulative infiltration capacity of soil covered by *Tamarix chinensis* Lour. was significantly higher than that of bare land and soil covered by *Suaeda glauca* (*Bunge*) Bunge. The accumulative infiltration capacities of the three vegetation covers indicated that the infiltration capacity of bare land was high at the soil surface layer but low in the deeper layer. There could be an obstacle horizon preventing soil water transportation. The existence of an obstacle horizon can directly influence soil salt eluviation, cause severe salt accumulation at the soil surface and inhibit plant growth and development. Plant growth has important effects both on soil salt and soil structure. The infiltration capacities of soils covered by *Tamarix chinensis* Lour. and *Suaeda glauca* (*Bunge*) Bunge. in the 10–20 cm and 20–30 cm soil layers are appreciably higher than that of bare land. Therefore, planting salt-tolerant plants can alter soil structure, increase water movement and salt eluviation, and it is an important measure for improvement of saline-alkaline soil (Zhang et al., 2007).

The depth of the wetting front is also an important indicator which could reflect soil water infiltration capacity. The dynamic change of wetting fronts in the layers for three vegetation covered soils showed that the changes of wetting fronts were the same as the accumulative infiltration in the 0–10 cm and 20–30 cm soil layers and differed in the 10–20 cm soil layer. Fig. 5 showed the dynamic change of the wetting

Table 2
Indicators of soil infiltration properties and salt content.

Plant cover	Soil layer (cm)	Accumulative infiltration (cm)	Initial infiltration rate (cm/min)	Stable infiltration rate (cm/min)	Total salt content (g/kg)
Bare land	0–10 cm	4.62a ± 1.08	0.983a ± 0.165	0.021a ± 0.009	28.21a ± 1.52
	10–20 cm	4.23a ± 0.76	0.950a ± 0.204	0.017a ± 0.004	18.59b ± 0.90
	20–30 cm	5.65a ± 1.70	0.567a ± 0.309	0.022a ± 0.008	16.31b ± 1.13
Suaeda glauca (*Bunge*) Bunge.	0–10 cm	4.10a ± 1.27	0.717a ± 0.484	0.020a ± 0.000	9.81a ± 0.40
	10–20 cm	5.48a ± 2.15	1.000a ± 0.300	0.020a ± 0.006	10.56a ± 1.21
	20–30 cm	4.60a ± 0.32	1.033a ± 0.330	0.027a ± 0.004	12.58a ± 1.43
Tamarix chinensis Lour.	0–10 cm	4.48b ± 0.68	0.617a ± 0.272	0.023a ± 0.012	15.38a ± 2.45
	10–20 cm	5.30ab ± 0.45	0.800a ± 0.082	0.028a ± 0.004	12.41a ± 1.25
	20–30 cm	6.70a ± 0.10	1.100a ± 0.100	0.033a ± 0.000	11.12a ± 1.00

a: $P < 0.01$; b: $P < 0.05$; c: no obvious difference.

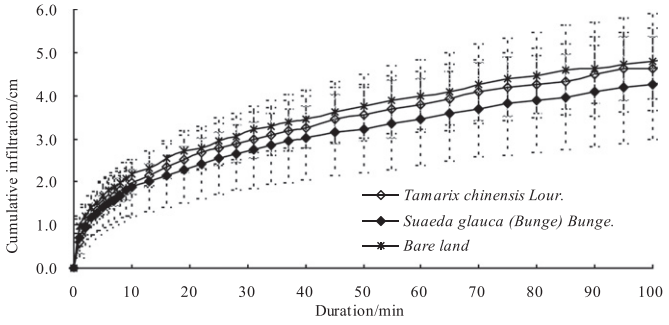

(a) 0-10cm

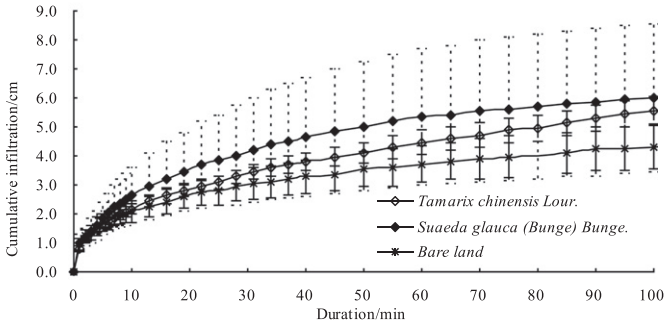

（b）10-20cm

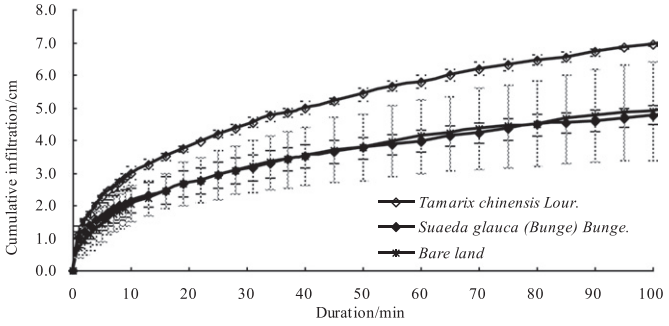

（c）20-30cm

Fig. 4. The dynamic accumulative infiltration capacity of soils with different vegetation covers.

front in the 10–20 cm soil layer of the soils with three vegetation covers. For soil covered by *Tamarix chinensis* Lour., although the total infiltration capacity was slightly lower than that of soil covered by *Suaeda glauca* (*Bunge*) Bunge., the wetting front depth was appreciably higher than those of bare land soil and soil covered by *Suaeda glauca* (*Bunge*) Bunge. This phenomenon indicates the high hydraulic conductivity of the soil covered by *Tamarix chinensis* Lour. Plant is the main factor which influences soil organic matter content, and the root system and its secretions can improve soil quality, including soil water conductivity, soil fertility, soil particle size and its proportion, also change the soil environment. Otherwise, *Tamarix chinensis* Lour. and *Suaeda glauca* (*Bunge*) Bunge. are all halophytes, their functions on soil salt include strong water absorption ability, salt accumulation by themselves then influence solute transportation in soil and change the salt distribution in soil profile.

3.1.2. Analysis of the capillary water absorption properties of marsh saline soil

As the deeper soil layers are closer to underground water and their hydraulic conductivities can directly influence the water and salt accumulation and storage of the upper soil layers, here we mainly focus on

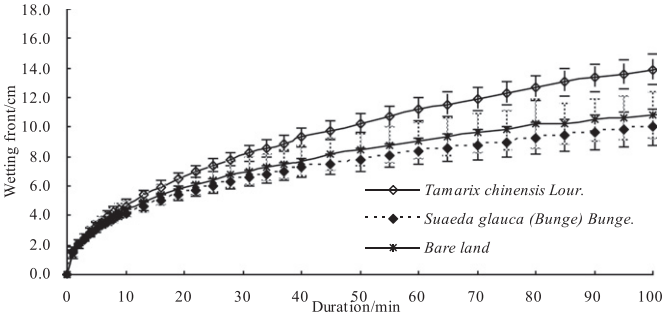

Fig. 5. The dynamics of the wetting fronts in the soils with three different vegetation covers.

the capillary water adsorption properties of soil covered by *Suaeda glauca* (*Bunge*) Bunge. in layers to analyze the soil capillary water adsorption characteristics.

Fig. 6 shows the dynamic change of accumulative capillary absorbed water volume, absorption rate and wetting front at each layer of *Suaeda glauca* (*Bunge*) Bunge. covered soil. The accumulative capillary absorbed water volume at each layer showed the same trends but differed in quantity within the same period (Fig. 6a). The accumulative capillary absorbed water volume increased with depth: highest in the 40–50 cm soil layer, followed by the 30–40 cm and 20–30 cm soil layers, and lowest in the 0–10 cm and 10–20 cm soil layers, with a relatively consistent trend. At 100 min, the accumulative capillary absorbed water volumes were 3.28, 3.34, 4.67, 6.98 and 7.32 cm from the soil surface to the deeper layers. The capillary water rise rate of each layer is shown in Fig. 6b. Within 1 min after the start of absorption, the absorption rate of each soil layer was 1.15, 1.27, 1.27, 1.60 and 2.45 cm/min from the soil surface (0–10 cm) to the deepest layer (40–50 cm). During the whole absorption process, the capillary water rise rates of the 30–40 cm and 40–50 cm soil layers were appreciably faster than those of the other soil layers. The decreases in the rates of these two layers were relatively slow, declining to 0.09 cm/min at 85 min. The rate declined to 0.09 cm/min for the 20–30 cm soil layer at 40 min and to the same rate for the 0–20 cm soil layer at approximately 20 min. The property that capillary water rises fast and declines slowly is extremely beneficial to the upward movement of underground water and the upward movement and accumulation of salt at the soil surface. The dynamic change of wetting front (Fig. 6c) was the same as that of the accumulative capillary absorbed water volume. The height of the capillary water rise of the deeper soil layer was evidently higher than that of the other soil layers during the same period, reflecting the strong water absorption capacity and hydraulic conductivity of the deeper soil layers. This may be due to greater sand content in deeper soil layer.

Table 3 shows the accumulative capillary absorbed water volume and infiltration rate during different time periods of the soils with three vegetation covers. In Table 3, the data at 1 min and 90 min were selected to represent the capillary absorption characteristics at the initial and stable stages, respectively. In the 0–10 cm soil layer of soil covered by *Tamarix chinensis* Lour., the rates of capillary water rise at both the initial and end stages were higher than those of the other two soils; the capillary absorbed water volume and height of capillary water rise were relatively high (Table 3). In the 10–20 cm soil layer, the capillary water absorption rate, height of capillary water rise and capillary absorbed water volume of soil covered by *Suaeda glauca* (*Bunge*) Bunge. and bare land were significant higher than those of soil covered by *Tamarix chinensis* Lour. At the initial stage in the 20–30 cm soil layer, the rates of capillary water rise of soils covered by *Suaeda glauca* (*Bunge*) Bunge. and *Tamarix chinensis* Lour. were similar, but they were lower than that of bare land. The stable capillary water absorption rates of the three soils were the same. During the stable infiltration period, the height of capillary water rise and accumulative absorbed water volume were highest in soil covered by *Tamarix chinensis* Lour., followed by those in soil covered by *Suaeda glauca*

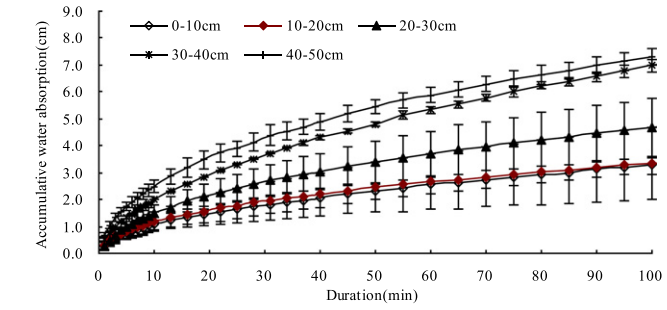

（a）Accumulative volume of capillary absorption water

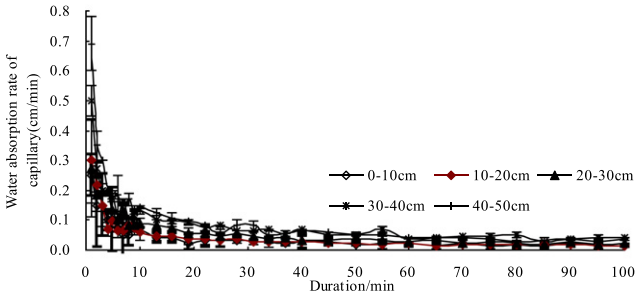

（b）Capillary water rise rate

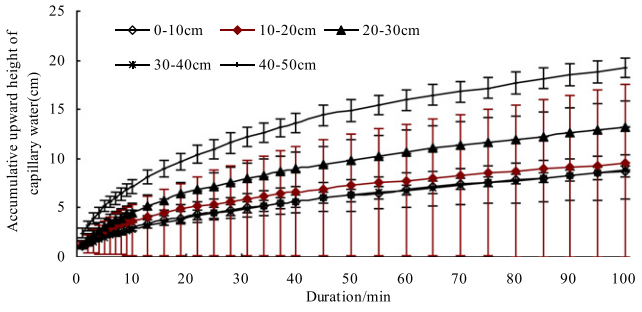

(c)Accumulative height of capillary water

Fig. 6. The capillary accumulative absorbed water volume and capillary water rise rate of soil covered by *Suaeda glauca* (*Bunge*) Bunge.

(*Bunge*) Bunge., and lowest for bare land. From this, we can conclude that halophytes can improve soil water transportation characteristics.

3.2. Dynamic simulation of the one-dimensional ponding infiltration process and the capillary water absorption process in saline soil

The theories and methods of simulating the dynamics of water infiltration of non-saline soil were well-studied and completed. The most classic model was the Green-Ampt infiltration model, which was proposed earlier and was the focus of much work to promote, apply and improve it. Other common models, including the Philip formula, the Kostiakov two-parameter model, the Kostiakov-Lewis three-parameter model, and the Horton infiltration equation, were also frequently used.

This study employed the Philip model, the Kostiakov two-parameter model and the Kostiakov-Lewis model to simulate the dynamics of the infiltration rate of soils with three vegetation covers. The Kostiakov two-parameter model ($i(t) = kt^{-\alpha}$) simulated the one-dimensional infiltration process and the dynamics of capillary water absorption best, which was consistent with other publications (Yin et al., 2007; Wu and Wang, 2007). Table 4 shows the simulated dynamics of ponding infiltration rate and capillary water rise rate.

Table 4 shows that the determination coefficients (R^2) of each soil layer were higher than 0.8, indicating the good performance of the model. By comparing the determination coefficients of the ponding infiltration process and the capillary water absorption process of soil layers of the same depth, the determination coefficient of capillary water absorption was revealed to always be higher than that of the ponding infiltration process, indicating that the Kostivkov two-parameter model was better for simulating the capillary water absorption process of saline soil.

3.3. Relationship between the one-dimensional ponding infiltration properties and capillary water absorption properties of saline soil

3.3.1. Comparison of the water transportation rate between ponding infiltration and capillary absorption processes

To analyze the characteristics of the two water transportation processes, the water transportation rates of the ponding infiltration process and the capillary water absorption process were compared. The results are shown in Table 5. The initial capillary water rise rates (ICWRs) were lower than the initial infiltration rate (IIR). The ICWR of bare land increased with soil layer depth, otherwise, its IIR decreased. The ratio of IIR to ICWR decreased from 5.129 in 0–10 cm layer to 2.100 in 20–30 cm layer. For the soil covered by *Suaeda glauca* (*Bunge*) Bunge., the initial capillary water rise rate of 10–20 cm layer was the highest, and other layers is lower. Initial infiltration rate, the ratio of infiltration rate to the initial capillary water rise rate tended to increase with soil layer depth. ICWR of soil covered by *Tamarix chinensis* Lour. decreased with soil layer depth increasing, and infiltration increased, IIR/ICWR also increased with soil layer depth. The stable water transportation rate of ponding infiltration and capillary water adsorption did not show out obvious principle.

As in all, initial infiltration rate was high, and it decreased rapidly, difference between initial infiltration rate and stable infiltration rate was large, the change of infiltration capability was obvious. Then, for capillary water adsorption, variation amplitude of capillary water adsorption rate was more stable during whole experimental process relatively.

The reasons could be the impact of saline ions and the soil expansion properties after water absorption. The marsh saline soil in the Yellow

Table 3
Indicators of the capillary water absorption characteristics of the soils with three vegetation covers.

Soil layer (cm)	Duration (min)	Water absorption rate of capillary (cm/min)			Accumulative height of capillary water (cm)			Accumulative volume of capillary absorption water (cm)		
		Bare land	*Suaeda glauca* (*Bunge*) Bunge.	*Tamarix chinensis* Lour.	Bare land	*Suaeda glauca* (*Bunge*) Bunge.	*Tamarix chinensis* Lour.	Bare land	*Suaeda glauca* (*Bunge*) Bunge.	*Tamarix chinensis* Lour.
0–10	1	0.192a ± 0.096	0.233a ± 0.047	0.270a ± 0.128	0.97a ± 0.25	1.23a ± 0.12	1.17a ± 0.61	0.19a ± 0.10	0.23a ± 0.05	0.27a ± 0.13
	90	0.015a ± 0.009	0.025a ± 0.005	0.022a ± 0.002	8.55a ± 3.93	7.90a ± 0.65	9.55a ± 2.51	2.80a ± 1.57	4.28a ± 1.65	3.47a ± 1.03
10–20	1	0.200a ± 0.122	0.300a ± 0.141	0.250a ± 0.050	1.20a ± 0.36	1.27a ± 0.34	0.87a ± 0.05	0.25a ± 0.12	0.30a ± 0.14	0.19a ± 0.10
	90	0.008a ± 0.008	0.020a ± 0.006	0.013a ± 0.005	8.25a ± 3.63	9.13a ± 3.44	6.95a ± 0.39	2.78a ± 1.47	3.19a ± 1.26	2.15a ± 0.50
20–30	1	0.270a ± 0.037	0.273a ± 0.164	0.250a ± 0.147	1.37a ± 0.29	1.27a ± 0.41	1.23a ± 0.37	0.27a ± 0.04	0.27a ± 0.16	0.25a ± 0.15
	90	0.023a ± 0.013	0.021a ± 0.001	0.033a ± 0.001	11.93a ± 2.92	12.60a ± 2.57	14.28a ± 2.49	4.15a ± 1.30	4.46a ± 1.05	5.12a ± 0.92

a: $P < 0.01$; b: $P < 0.05$; c: no obvious difference.

Table 4
Simulated dynamics of soil ponding infiltration rate and capillary water rise rate.

Plant cover	Soil layer (cm)	Infiltration			Capillary absorption		
		k	α	R square	k	A	R square
Bare land	0–10	0.490	0.764	0.8757	0.224	0.616	0.9665
	10–20	0.511	0.834	0.8539	0.180	0.620	0.7844
	20–30	0.719	0.826	0.9247	0.281	0.561	0.9364
Suaeda glauca (*Bunge*) Bunge.	0–10	0.404	0.716	0.9266	0.226	0.583	0.9219
	10–20	0.791	0.837	0.9212	0.257	0.623	0.9677
	20–30	0.455	0.734	0.9195	0.333	0.591	0.9694
Tamarix chinensis Lour.	0–10	0.542	0.785	0.8607	0.239	0.561	0.9654
	10–20	0.456	0.669	0.8995	0.164	0.606	0.9335
	20–30	0.720	0.744	0.9498	0.345	0.552	0.9612

River Delta was high in salt content (Table 1). The main cation is Na^+. Under the conditions of ponding infiltration, the existence of Na^+ makes soil scatter into tiny particles easily, forming soil crust and blocking soil pores. The shrinking of soil pores after soil expansion resulted in the inhibition of water leaching and water adsorption (Yousaf et al., 1987; Shainberg, 1981a, b; Jayawardane et al., 2011). The other possibility could be that the air in the soil pores blocked the leaching of water. During ponding infiltration, air in soil pores has support action to water, just like air resistance, water displaced air downwards and resisted by air oppositely, soil air cannot be expelled so that water could not infiltrate into soil layer smoothly.

During capillary water absorption, because the soil was relatively dry at the beginning, the absorption capacity of the soil surface was strong (Datry et al., 2004; Fernández-Gálvez et al., 2007). With the help of strong capillary forces and surface tension, water can rapidly rise in the capillaries. As the capillary water rises, water replaced soil air from the bottom to the top, which was in accordance with the tendency of the movement of air with less resistance, resulting in more stable water transportation, but with the increase of capillary water volume, the gravity may become an obstacle (Peck, 1965).

3.3.2. The relationship between ponding infiltration and the accumulative infiltration capacity and wetting front during the capillary water absorption process

During the ponding infiltration process of non-saline soil, there was a linear relationship between the wetting front and the accumulative infiltration capacity, i.e., $I = (\theta_s - \theta_i)x_f = \Delta\theta x_f$, where I is the accumulative infiltration capacity (cm), x_f is the distance of the advance of the wetting front (cm), and θ_s and θ_i are saturated soil water content and initial soil water content (cm^3/cm^3), respectively. The linear simulated results of the relationship between the accumulative infiltration capacity and the wetting front, as well as between the accumulative capillary absorbed water volume and the height of capillary water rise, are shown in Table 6.

According to Table 6, there were significant linear relationships between the wetting front and the accumulative infiltration capacity and between the height of capillary water rise and the accumulative capillary absorbed water volume during the ponding infiltration and capillary water absorption processes, with determination coefficients larger than 0.8. The linear relationship between the height of capillary water rise and the accumulative capillary absorbed water volume during the absorption process was much stronger than that in the ponding infiltration process, with a determination coefficient larger than 0.99. Additionally, the value of $\Delta\theta$ showed that the change in the water content in the 10–20 cm soil layer was 0.627 in soil covered by *Suaeda glauca* (*Bunge*) Bunge. and 0.543 in soil covered by bare land. The values were obviously large and severely departed from reality. Thus, they could not simulate the actual changes in soil water content during infiltration. The simulated results of capillary water absorption showed that $\Delta\theta$ ranged between 0.30 and 0.37, which was consistent with reality. This showed that the one-dimensional linear model can well-simulate the relationship between the accumulative capillary absorbed water volume and the height of capillary water rise better.

4. Conclusions

The dynamic changes of wetland saline soil infiltration and capillary water absorption were accordance with common principle. The initial infiltration rate increased with soil depth in the soils covered by *Suaeda glauca* (*Bunge*) Bunge. and *Tamarix chinensis* Lour. Although the infiltration capacity of bare land was very strong in the surface layer, but it was lower in deeper layers, which may directly impacts soil salt eluviation and results in relatively severe salt accumulation at the soil surface. For soil covered by *Suaeda glauca* (*Bunge*) Bunge. and *Tamarix chinensis* Lour., infiltration rates in the 10–20 cm and 20–30 cm layers were very strong. Deeper wetting front of *Tamarix chinensis* Lour. covered soil, indicated its advantages in water conduction and transportation. Therefore, planting salt-tolerant plants is an important measure of salt eluviation and saline-alkaline soil improvement.

The initial rate of capillary water rise of soils covered by different vegetation types showed an increasing trend from the surface layer to deeper layers. However, this pattern of changes with soil depth was extremely weak. The mechanical composition and total salt content, but not soil depth, were the main factors affecting the soil infiltration capacity.

Comparing the water transportation rate during ponding infiltration and capillary water absorption revealed that the initial rate of capillary water rise was lower than the initial infiltration rate. But infiltration rate decreased more rapidly than capillary water adsorption rate. Therefore, controlling the underground water table and cutting off the capillary interactions between the upper and lower layers of the soil were also important for controlling salt accumulation.

Theories and methods about simulating the infiltration processes of ordinary non-saline soil can also be applied to dynamic simulation of the ponding infiltration and capillary absorption of saline soil.

There were significant linear relationships between the accumulative infiltration capacity and the wetting front during infiltration and between the accumulative capillary absorbed water volume and the height of capillary water rise during capillary water absorption. The

Table 5
Comparison of ponding infiltration rates and capillary water rise rates.

Plant cover	Soil layer (cm)	Initial capillary water rise rate (cm/min)	IIR (cm/min)	IIR/ICWR	Stable capillary water rise rate (cm/min)	Stable infiltration rate (cm/min)
Bare land	0–10	0.192a ± 0.096	0.983a ± 0.165	5.129	0.022a ± 0.011	0.022a ± 0.009
	10–20	0.200a ± 0.122	0.950a ± 0.204	4.750	0.017a ± 0.014	0.017a ± 0.004
	20–30	0.270a ± 0.037	0.567a ± 0.309	2.100	0.026a ± 0.013	0.022a ± 0.008
Suaeda glauca (*Bunge*) Bunge.	0–10	0.233a ± 0.047	0.717a ± 0.484	2.868	0.025a ± 0.001	0.020a ± 0.000
	10–20	0.300a ± 0.141	1.000a ± 0.300	3.333	0.022a ± 0.007	0.019a ± 0.006
	20–30	0.273a ± 0.164	1.033a ± 0.330	3.779	0.024a ± 0.006	0.027a ± 0.004
Tamarix chinensis Lour.	0–10	0.270a ± 0.128	0.617a ± 0.272	2.285	0.023a ± 0.009	0.023ab ± 0.012
	10–20	0.250a ± 0.050	0.800a ± 0.082	4.286	0.013a ± 0.006	0.029b ± 0.004
	20–30	0.250a ± 0.147	1.100a ± 0.100	4.400	0.033a ± 0.006	0.033a ± 0.000

ICWR: initial capillary water rise rate, cm/min; IIR: initial infiltration rate, cm/min.

Table 6
Linear simulated results of the relationship between the wetting front and accumulative infiltration capacity and between the height of capillary water rise and the accumulative capillary absorbed water volume.

Plant cover	Soil layer (cm)	Infiltration		Capillary absorption	
		$\Delta\theta$	R square	$\Delta\theta$	R square
Bare land	0–10	0.418	0.9678	0.321	0.9958
	10–20	0.421	0.9655	0.333	0.9946
	20–30	0.543	0.9874	0.338	0.9930
Suaeda glauca (*Bunge*) Bunge.	0–10	0.387	0.9763	0.368	0.9959
	10–20	0.627	0.9958	0.339	0.9951
	20–30	0.415	0.9736	0.345	0.9960
Tamarix chinensis Lour.	0–10	0.415	0.9925	0.358	0.9962
	10–20	0.408	0.9833	0.348	0.9971
	20–30	0.419	0.9887	0.350	0.9959

linear relationship between the capillary absorbed water volume and the height of capillary water rise during capillary water absorption was much more significant.

Acknowledgement

This work was supported by the Project of the Cultivation Plan of Superior Discipline Talent Teams of Universities in Shandong Province: "the Coastal Resources and Environment team for Blue-yellow Area", the National Natural Science Foundation of China (41471223 and 41271236), and the Natural Science Foundation of Shandong Province (ZR2013DM010 and ZR2014JL026).

References

Abu-Sharar, T.M., Bingham, F.T., Rhoades, J.D., 1987. Reduction in hydraulic conductivity in relation to clay dispersion and disaggregation. Soil Sci. Soc. Am. J. 51, 342–346.
Agassi, M., Shainberg, I., Morin, J., 1981. Effect of electrolyte concentration and soil sodicity on infiltration rate and crust formation. Soil Sci. Soc. Am. J. 45, 848–851.
Ayars, J.E., Hutmacher, R.B., Schoneman, R.A., Vale, S.S., Pflaum, T., 1993. Longterm use of saline water for irrigation. Irrig. Sci. 14, 27–34.
Bagarello, V., Iovino, M., Palazzolo, E., Panno, M., Reynolds, W.D., 2006. Field and laboratory approaches for determining sodicity effects on saturated soil hydraulic conductivity. Geoderma 130, 1–13.
Bardhan, G., Russo, D., Goldstein, D., Levy, G.J., 2016. Changes in the hydraulic properties of a clay soil under long-term irrigation with treated wastewater. Geoderma 264, 1–9.
Barzegar, A.R., Youse, A., Daryashenas, A., 2002. The effect of addition of different amounts and types of organic materials on soil physical properties and yield of wheat. Plant Soil 24 (7), 295–301.
Callaghan, M.V., Cey, E.E., Bentley, L.R., 2014. Hydraulic conductivity dynamics during salt leaching of a sodic structured subsoil. Soil Sci. Soc. Am. J. 78, 1563–1574.
Churchman, G.J., Skjemstad, J.O., Oades, J.M., 1993. Influence of clay minerals and organic matter on effects of sodicity on soils. Aust. J. Soil Res. 31, 779–800.
Crescimanno, G., Iovino, M., Provenzano, G., 1995. Influence of salinity and sodicity on soil structural and hydraulic characteristics. Soil Sci. Soc. Am. J. 59, 1701–1708.
Datry, T., Malard, F., Gibert, J., 2004. Dynamics of solutes and dissolved oxygen in shallow urban groundwater below a stormwater infiltration basin. Sci. Total Environ. 329, 215–229.
Fernández-Gálvez, J., Barahona, E., Iriarte, A., Mingorance, M.D., 2007. A simple methodology for the evaluation of groundwater pollution risks. Sci. Total Environ. 378, 67–70.
Frenkel, H., Goertzen, J.O., Rhoades, J.D., 1978. Effects of clay type and content, exchangeable sodium percentage, and electrolyte concentration on clay dispersion and soil hydraulic conductivity. Soil Sci. Soc. Am. J. 42, 32–39.
Jayawardane, N.S., Christen, E.W., Arienzo, M., Quayle, W.C., 2011. Evaluation of the effects of cation combinations on soil hydraulic conductivity. Soil Res. 49, 56–64.
Kazman, Z., Shainberg, I., Gal, M., 1983. Effect of low levels of exchangeable Na and applied phosphogypsum on the infiltration rate of various soils. Soil Sci. 135, 184–192.
Levy, G.J., Goldstein, D., Mamedov, A.I., 2005. Saturated hydraulic conductivity of semiarid soils: combined effects of salinity sodicity and rate of wetting. Soil Sci. Soc. Am. J. 69, 653–662.
Moutier, M., Shainberg, I., Levy, G.J., 1998. Hydraulic gradient, aging and water quality effects on hydraulic conductivity of a vertisol. Soil Sci. Soc. Am. J. 62, 1488–1496.
Pardini, G., Gispert, M., Dunjo, G., 2003. Runoff erosion and nutrient depletion in five Mediterranean soils of NE Spain under different land use. Sci. Total Environ. 309, 213–224.
Peck, A.J., 1965. Moisture profile development and air compression during water uptake by bounded porous bodies: 3. Vertical columns. Soil Sci. 100, 44–51.
Quirk, J.P., Schofield, R.K., 2013. Landmark papers: no.2. The effect of electrolyte concentration on soil permeability. Eur. J. Soil Sci. 64, 2–15.
Reading, L.P., Baumgartl, T., Bristow, K.L., Lockington, D.A., 2012. Hydraulic conductivity increases in a sodic clay soil in response to gypsum applications: impacts of bulk density and cation exchange. Soil Sci. 177, 165–171.
Shainberg, I., Rhoades, J.D., Prather, R.J., 1981a. Effect of low electrolyte concentration on clay dispersion and hydraulic conductivity of a sodic soil. Soil Sci. Soc. Am. J. 45, 273–277.
Shainberg, I., Rhoades, J.D., Suarez, D.L., Prather, R.J., 1981b. Effect of mineral weathering on clay dispersion and hydraulic conductivity of sodic soils. Soil Sci. Soc. Am. J. 45, 287–291.
Shao, M., Horton, R., 1999. Reply to comment on "Integral method for estimating soil hydraulic properties". Soil Sci. Soc. Am. J. 63 (2), 256.
Shi, W.J., Shen, B., Wang, Z.R., Wang, W.Y., 2007. Maximum height of upward capillary water movement in layered soil. Agric. Res. Arid Areas 25 (1), 94–97 in Chinese.
So, H.B., Aylmore, L.A.G., 1993. How do sodic soils behave? The effects of sodicity on soil physical behavior. Aust. J. Soil Res. 31, 761–777.
Suarez, D.L., Wood, J.D., Scott, M.L., 2006a. Effect of SAR on water infiltration under a sequential rain–irrigation management system. Agric. Water Manag. 86, 150–164.
Suarez, D.L., Wood, J.D., Lesch, S.M., 2006b. Effect of SAR on water infiltration under sequential rain-irrigation management system. Agric. Water Manag. 86, 150–164.
Turrion, M.B., Lopez, O., Lafuente, F., Mulas, R., Ruiper, C., Puyo, A., 2007. Soil phosphorus forms as quality indicators of soils under different vegetation covers. Sci. Total Environ. 378, 195–198.
Wu, Z.D., Wang, Q.J., 2007. Infiltration characteristics of brackish water by one dimensional algebraic model. Trans. Chin. Soc. Agric. Eng. 23 (06), 21–26 (in Chinese).
Yan, Y., Wang, Q.J., Fan, J., Zhao, J., 2007. Method for determining soil water and solute transport parameters using one soil column. J. Hydraul. Eng. 38 (1), 120–126 (in Chinese).
Yin, J., Fei, L.J., Cheng, D.J., 2007. Laboratory experiment on characteristics of capillary water upward movement from homogeneous soil. Trans. Chin. Soc. Agric. Eng. 23 (6), 91–94 (in Chinese).
Yousaf, M., Ali, O.M., Rhoades, J.D., 1987. Clay dispersion and hydraulic conductivity of some salt-affected arid land soils. Soil Sci. Soc. Am. J. 51, 905–907.
Zhang, L.B., Xu, H.L., Zhao, G.X., 2007. Salt tolerance of *Suaeda salsa* and its soil ameliorating effect on coastal saline soil. Soils 39 (2), 310–313 (in Chinese).